

# MK-SGN: A Spiking Graph Convolutional Network with Multimodal Fusion and Knowledge Distillation for Skeleton-based Action Recognition

Naichuan Zheng<sup>1</sup>, Hailun Xia<sup>1\*</sup>, Zeyu Liang<sup>1</sup> Yuanyuan Chai<sup>1</sup>

<sup>1</sup>Beijing Laboratory of Advanced Information Networks,  
Beijing Key Laboratory of Network System Architecture and Convergence,  
School of Information and Communication Engineering,  
Beijing University of Posts and Telecommunications,  
Beijing, China, 100876  
{2022110134zhengnaichuan, xiahailun, lzy\_sfading}@bupt.edu.cn, chaiyyliuky@163.com

## Abstract

In recent years, skeleton-based action recognition, leveraging multimodal Graph Convolutional Networks (GCN), has achieved remarkable results. However, due to their deep structure and reliance on continuous floating-point operations, GCN-based methods are energy-intensive. We propose an innovative Spiking Graph Convolutional Network with Multimodal Fusion and Knowledge Distillation (MK-SGN) to address this issue. By merging the energy efficiency of Spiking Neural Network (SNN) with the graph representation capability of GCN, the proposed MK-SGN reduces energy consumption while maintaining recognition accuracy. Firstly, we convert Graph Convolutional Networks (GCN) into Spiking Graph Convolutional Networks (SGN) establishing a new benchmark and paving the way for future research exploration. During this process, we introduce a spiking attention mechanism and design a Spiking-Spatio Graph Convolution module with a Spatial Global Spiking Attention mechanism (SA-SGC), enhancing feature learning capability. Secondly, we propose a Spiking Multimodal Fusion module (SMF), leveraging mutual information to process multimodal data more efficiently. Lastly, we delve into knowledge distillation methods from multimodal GCN to SGN and propose a novel, integrated method that simultaneously focuses on both intermediate layer distillation and soft label distillation to improve the performance of SGN. MK-SGN outperforms the state-of-the-art GCN-like frameworks on three challenging datasets for skeleton-based action recognition in reducing energy consumption. It also outperforms the state-of-the-art SNN frameworks in accuracy. Specifically, our method reduces energy consumption by more than 98% compared to typical GCN-based methods, while maintaining competitive accuracy on the NTU-RGB+D 60 cross-subject split using 4-time steps.

## Introduction

Human action recognition is essential for applications like human-robot interaction (Sheridan 2016), video surveillance (Elharrouss, Almaadeed, and Al-Maadeed 2021), and emergency detection (Agapiou et al. 2015). Depth sensors, with their robustness against complex backgrounds, have increased interest in skeleton-based action recognition (Chen et al. 2021b; Kim and Mnih 2018; Liu et al. 2020; Song, Lan, and Xing 2017). Graph Convolutional Networks (GCNs), a

type of ANN, have shown remarkable results (Nwakanma et al. 2021; Li et al. 2019a; Shi et al. 2019a). ST-GCN (Yan, Xiong, and Lin 2018) was the first to represent skeletons through spatio-temporal relations, inspiring many subsequent studies. Shift-GCN (Cheng et al. 2020) and CTR-GCN (Chen et al. 2021a) advanced lightweight processing. Multimodal integration enhances overall understanding and system performance by providing complementary information (Baltrušaitis, Ahuja, and Morency 2018; Gao et al. 2020). Recent methods train multiple unimodal GCNs to recognize human actions from various skeleton data modalities, such as joint, bone, and motion (Chen et al. 2021a; Chi et al. 2022; Yang et al. 2022). A multimodal foundation model, the HULK, further improved precision in skeleton-based action recognition (Wang et al. 2023). However, those methods have high computational energy consumption, especially for multimodal data. Even lightweight designs like Shift-GCN and CTR-GCN require  $46mJ$  and  $36.25mJ$  per action sample, respectively, while 2S-AGCN (Shi et al. 2019b) uses up to  $164.68mJ$  per sample. More details on the theoretical energy consumption of these models are discussed in the Appendix.

Spiking Neural Networks (SNN) are known for their event-driven characteristics, leading to low energy consumption (Roy, Jaiswal, and Panda 2019; Tavanaei et al. 2019). With advancements in artificial neural networks (ANNs), SNNs have improved their performance through advanced architectures (Hu, Tang, and Pan 2021; Hu et al. 2024). Examples include Spiking Graph Neural Networks, Spiking Recurrent Neural Networks (Veeriah, Zhuang, and Qi 2015), and Spiking Transformers (Zhou et al. 2022; Yao et al. 2024), all of which have been extensively researched. The current Spiking Neural Networks research focuses on RGB image classification and event-driven recognition (Zhang et al. 2022; Stromatias et al. 2017; Kim, Chough, and Panda 2022), achieving notable energy efficiency and accuracy. Inspired by this, we aim to explore skeletal action recognition using Spiking Graph Convolutional Networks, to reduce energy consumption and expand SNNs' potential applications in this dynamic scenario with high accuracy.

Several scientific challenges during this research process prompt deep reflection. How can we convert skeletal data with complex graphical characteristics into spike signals?

\*Corresponding Author

Furthermore, can the spike-form data be compatible with traditional GCN and function effectively in action recognition tasks? How should we design strategies to achieve effective data fusion within SNN when facing complex multimodal data? Lastly, how can we balance reducing energy consumption with maintaining recognition accuracy?

To tackle these issues, we first propose a spiking coding module to convert skeletal data into event spikes and introduce a spiking attention mechanism to construct a Spiking Graph Convolutional Network (SGN) for feature representation and classification. Based on this, we bridge the gap between SGN and traditional Graph Convolutional Networks (GCN) in terms of feature extraction and information propagation. Secondly, we innovatively develop a multimodal spike data fusion module based on mutual information, utilizing mutual information to compute the correlation between multimodal data for early fusion. This allows the model to leverage the complementary information from multimodal skeletal data fully and avoids the heavy training and testing burden brought by late-stage ensemble methods. Thirdly, we propose a novel GCN-to-SGN knowledge distillation method, leveraging the high precision of traditional GCN to guide the training of SGN. This method implements the distillation of features from intermediate layers and soft labels, improving model accuracy without increasing model complexity. Given the maturity of GCN networks and the availability of numerous pre-trained weights, this process imposes no additional training burden. Ultimately, we propose a Spiking Graph Convolutional Network with Multimodal Fusion and Knowledge Distillation (MK-SGN), pioneering the introduction of SNN into the field of skeleton-based action recognition. In summary, our work has three main contributions as follows:

(1) We develop a novel MK-SGN, introducing skeleton-based action recognition into a new research domain through Spiking Neural Networks (SNN). This approach addresses the previously overlooked issue of energy consumption and sets a new benchmark for energy efficiency while maintaining recognition accuracy.

(2) We propose a Spiking Multimodal Fusion (SMF) module for fusing multimodal data based on mutual information to reduce energy consumption while enhancing performance.

(3) We innovatively propose a knowledge distillation method from GCN to SGN, achieving both intermediate layer and soft label distillation for heterogeneous networks. Specifically, we design a Feature Translation Module (FTM) to convert intermediate layer features from multimodal GCN into spike-form features for intermediate layer distillation.

(4) Extensive experiments on two challenging datasets demonstrate the advantages of our work. The theoretical energy consumption of MK-SGN is 0.614 mJ per action sample. Compared to state-of-the-art GCN-based methods, it reduces energy consumption by more than 98%. Moreover, we surpass the accuracy of state-of-the-art SNN-based methods.

## Related Work

In recent years, deep learning has significantly advanced skeleton-based action recognition. Early methods utilized

CNNs (Chéron, Laptev, and Schmid 2015; Liu, Liu, and Chen 2017) and RNNs (Liu et al. 2017; Wang and Wang 2017), while ST-GCN (Liu et al. 2016) introduced graph representations to capture spatio-temporal relationships. Subsequent studies have focused on enhancing GCN performance (Feng, Zhao, and Zhao 2022). For example, AS-GCN (Li et al. 2019b) captures global and local information, while Shift-GCN (Cheng et al. 2020) significantly reduces computational complexity while improving accuracy. Multimodal skeletal data, including joint, bone, and motion information, has also garnered attention, as seen in CTR-GCN (Chen et al. 2021a) and Info-GCN (Chi et al. 2022). Hulk leveraged multimodal pretrained large models to achieve new advancements (Wang et al. 2023). However, most studies have focused on ANNs, prioritizing accuracy over energy efficiency. This work is the first to convert skeleton-based action recognition from ANNs to SNNs, addressing energy consumption issues. Unlike ANNs, SNNs transmit information via discrete spike sequences, inspired by biological principles (Shrestha and Orchard 2018). This mode mimics brain function, offering significant potential for energy reduction (Lee et al. 2020a). Early research focused on designing spiking neurons to transform continuous inputs into spike sequences, such as the Leaky Integrate-and-Fire (LIF) model neuron (Wu et al. 2018; Dutta et al. 2017). The dynamic model of LIF is described as:

$$\tau_m \frac{dV}{dt} = -(V - V_{\text{rest}}) + R \cdot I(t) \quad (1)$$

where  $V(t)$  represents the membrane potential at the current time point, where  $V_{\text{rest}}$  denotes the neuron’s resting potential.  $I(t)$  indicates the input current. The membrane time constant is given by  $\tau_m$ , and  $V_{\text{thresh}}$  is the threshold potential that triggers the firing of an action potential. After firing, the membrane potential is reset to  $V_{\text{reset}}$ . The model’s discrete update time step is  $\Delta t$ . The update of the membrane potential can be written as follows:

$$V(t+\Delta t) = \begin{cases} V_{\text{reset}}, & \text{if } V(t) \geq V_{\text{thresh}} \\ V(t) + \left( \frac{-V(t) - V_{\text{rest}} + I(t)}{\tau_m} \right) \Delta t, & \text{otherwise} \end{cases} \quad (2)$$

With the advancement of ANN frameworks, research has begun to explore utilizing existing ANN architectures and weights for SNN design. A key focus is addressing differences in backpropagation between spiking networks and ANNs (Xiao et al. 2021; Lee, Delbruck, and Pfeiffer 2016; Lee et al. 2020b). More studies are devoted to designing ways to replace activation layers in traditional networks with spiking neurons, as events composed of 0s and 1s cannot be used to compute gradients. These studies include Spiking Graph Convolutional Networks (SGCNs) (Zhu et al. 2022), Spiking Transformers (Zhou et al. 2022; Yao et al. 2024), Spiking Recurrent Neural Networks (SRNNs) (Lotfi Rezaabad and Vishwanath 2020) and Spiking Convolutional Neural Networks (SCNNs) (Hu, Tang, and Pan 2021; Hu et al. 2024). Existing SNN research involves traditional ANN tasks, with many studies focusing on Transformer models for processing RGB images and achieving significant progress (Hu et al. 2023; Lin et al. 2022). Some researches

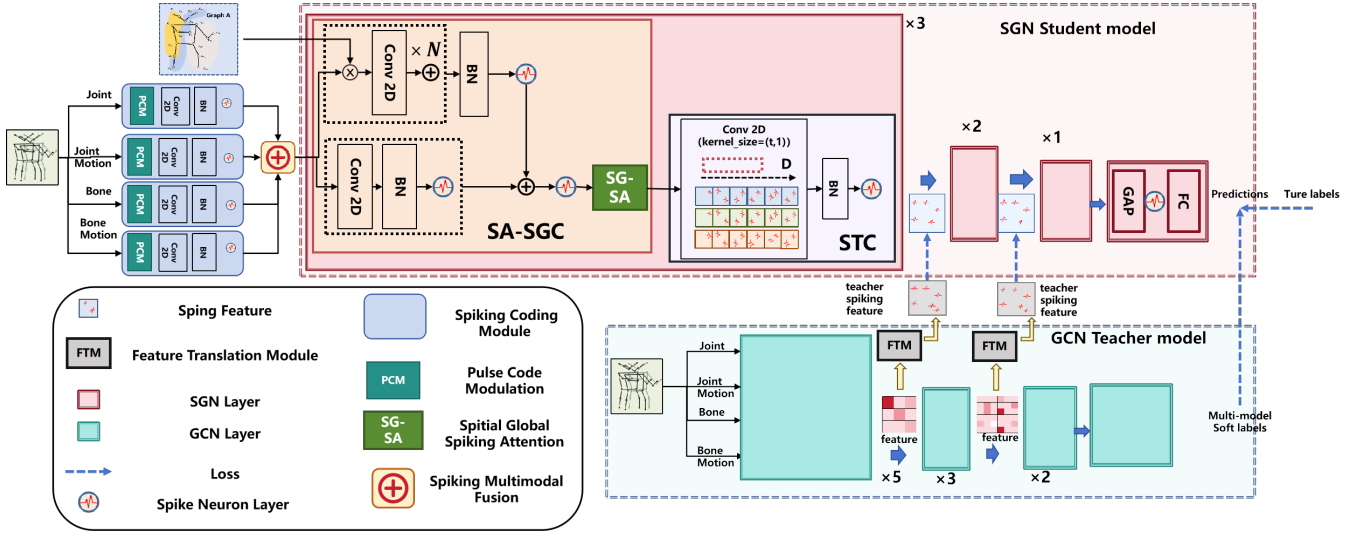


Figure 1: The overview of Spiking Graph Convolutional Network with Multimodal Fusion and Knowledge Distillation (MK-SGN).

concentrate on event-driven recognition (Zhang et al. 2022; Yao et al. 2021). However, research on SNN on skeleton-based action recognition remains relatively scarce.

## METHODOLOGY

We propose MK-SGN, a novel combination of SNN and GCN for skeleton-based action recognition. First, we introduce a Spiking Coding mechanism to convert skeleton sequence data into spike-form features and propose the foundational SGN network for classification. Then, we present a Spiking Multimodal Fusion module based on mutual information. Finally, we propose a multimodal GCN-to-SGN distillation method.

Our network architecture, illustrated in Figure 1, comprises a 10-layer multimodal teacher GCN network (Nwakanma et al. 2021; Li et al. 2019a) and a 6-layer SNN student network. The teacher network predicts the four multimodal skeleton data separately, and the final prediction results are fused after the Global Average Pooling (GAP) and Fully Connected (FC) layers to form soft labels. The student network fuses spike-form feature from multimodal data by mutual information in the Spiking Multimodal Fusion (SMF) module. Each layer of the student network consists of a SA-SGC module and a Spiking Temporal Convolution (STC) module. Our method implements intermediate features and soft label distillation in the knowledge distillation process. The intermediate features of the GCN teacher network are transformed into spike-form feature via the Feature Translation Module (FTM) to guide the training of the student SNN network. More details will be described as follows.

### Spiking Coding and the core of MK-SGN

In this chapter, we discuss how to convert continuous real numbers into spike representations. We then introduce the core of MK-SGN.

**Skeleton Spiking Coding** For a given 2D skeleton sequence data  $X \in \mathbb{R}^{C \times T \times V}$ , we utilize the Spiking Coding (SC) Module to convert it into spike-form features. The whole process can be written as follows:

$$P_0 = \text{PCM}(X) \quad (3)$$

$$P = \text{SN}(\text{BN}(\text{Conv2d}(P_0))), \quad P \in \mathbb{R}^{\text{Times} \times N \times V} \quad (4)$$

The Pulse Code Modulation (PCM) module increases the temporal resolution of the skeleton data by expanding its dimensions. Specifically, PCM converts continuous features into discrete spike signals, adding a temporal dimension. It maps the temporal window size  $T$  and the number of channels  $C$  into an  $N$ -dimensional temporal spiking sequence vector while retaining the joint nodes  $V$  with the graph structure.

A 2D convolution layer (Conv2d) with a kernel size of 3, followed by Batch Normalization (BN) and Spiking Neuron (SN) layers, aims to achieve a deep representation of the base signals. At this point, the dimension Times no longer represents the original  $T$  but rather the temporal dimension of the spiking signals.

**The Core** Revisiting traditional skeleton-based action recognition based on GCN, we now construct our SGN using features converted into the spike-form and adjacency matrices. Its process can be summarized as follows:

$$S = \tilde{D}^{-\frac{1}{2}} \tilde{A} \tilde{D}^{\frac{1}{2}} \quad (5)$$

where  $S$  is the normalized adjacency matrix,  $\tilde{A} = A + I$  denotes the sum of the adjacent matrix  $A$  and self-connection  $I$ .  $\tilde{D}$  is the diagonal degree matrix of  $\tilde{A}$ . Then, we calculate the graph convolutional output according to the following formula:

$$H = S^K P, H \in \mathbb{R}^{\text{Times} \times N \times V} \quad (6)$$

where  $H$  represents the output of early spatial spiking graph convolution,  $K$  is the number of graph convolutional layers.

Then the first layer of spatial graph convolution (SGC) can be written as:

$$H_0 = \text{SN}(P) + \text{SN}(HW^{(0)}) \quad (7)$$

where  $W^{(0)} \in \mathbb{R}^{N \times N'}$  is learnable parameters of the first layer. Each layer has its corresponding learnable weights, which we denote as  $W^{(l)} \in \mathbb{R}^{N^l \times N^{l+1}}$ .

We follow existing spiking attention methods (Zhou et al. 2022), using  $QKV$  with a pure spiking structure through SN and incorporating scaling factors  $s$  to control the large value of the matrix multiplication result. The process of computing the corresponding Spatial Global Spiking Attention (SG-SA) is as follows:

$$Q^{(0)} = \text{SN}_Q \left( \text{BN} \left( H_0 W_Q^{(0)} \right) \right), K^{(0)} = \text{SN}_K \left( \text{BN} \left( H_0 W_K^{(0)} \right) \right) \quad (8)$$

$$V^{(0)} = \text{SN}_V \left( \text{BN} \left( H_0 W_V^{(0)} \right) \right) \quad (9)$$

$$H_{SA}^{(0)} = H_0 + \text{SN} \left( Q^{(0)} K^{(0)T} V^{(0)} * s \right) \quad (10)$$

Based on the spiking attention mechanism, we propose a Spiking-Spatio Graph Convolution module with a Spatial Global Spiking Attention mechanism (SA-SGC) as illustrated in Figure 1.

After that, the first layer of Spiking-Temporal Convolution (STC) can be written as:

$$T^{(0)} = \text{SN} \left( \text{BN} \left( \text{Con2d} \left( H_{SA}^{(0)} \right) \right) \right) + \text{SN} \left( H_{SA}^{(0)} \right) \quad (11)$$

$$H_{SA}^{(l)} = \text{SN} \left( T^{(l-1)} \right) + \text{SN} \left( H_{SA}^{(l-1)} W^{(l-1)} \right) \quad (12)$$

$$T^l = \text{SN} \left( \text{BN}^{(l)} \left( \text{Con2d}^{(l)} \left( H_{SA}^{(l)} \right) \right) \right) + \text{SN} \left( H_{SA}^{(l)} \right) \quad (13)$$

In the end, the processed feature will be sent to GAP and FC to output the prediction as follows:

$$y = \text{FC} \left( \text{SN} \left( \text{GAP} \left( T^{(l)} \right) \right) \right) \quad (14)$$

where  $y \in \mathbb{R}^J$  and  $J$  is the number of action classes. Based on this, a standard cross-entropy loss is adopted for model optimization, as formulated as

$$L_b = -\frac{1}{B} \sum_{i=1}^B \sum_{j=1}^J Y_{ij} \log y_{ij} + (1 - Y_{ij}) \log (1 - y_{ij}) \quad (15)$$

where  $Y$  is the ground-truth label and  $B$  denotes the number of training samples.

### The spiking multimodal fusion module (SMF)

In this chapter, building upon the SC module and Foundational SGN discussed in the previous chapter, we describe how to fuse multimodal features. Skeletal data consists of four modalities: bones ( $X_B$ ), joints ( $X_J$ ), bone motions ( $X_{BM}$ ), and joint motions ( $X_{JM}$ ), all represented as  $X \in \mathbb{R}^{C \times T \times V}$ .

As shown in Figure 2, the SMF module implements early fusion based on mutual information to utilize multi-modal

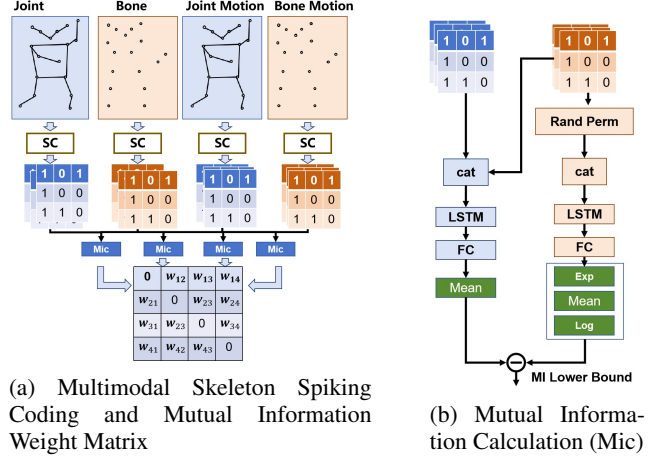


Figure 2: Multimodal Skeleton Spiking Coding and Mutual Information Weight Matrix Calculation Process

data and avoid the additional computing overhead and energy consumption that late fusion causes.

In the SMF, we first encode the multimodal data through the SC module separately to obtain their spike-form features: bones ( $P_B$ ), joints ( $P_J$ ), bone motions ( $P_{BM}$ ), and joint motions ( $P_{JM}$ ), all represented as  $P \in \mathbb{R}^{Times \times D \times N}$ , as shown in Figure 2a. These spike-form features are pairwise selected and concatenated along the dimension  $D$  to form a joint distribution. Then, one of the two spikes is randomly shuffled along the temporal dimension  $Times$ , and the same concatenation is performed to construct a marginal distribution. We employ an LSTM network and fully connected layers to build a mutual information prediction network and calculate the lower bound of mutual information as Figure 2b. We take bone data and joint data as examples, and the process can be described as follows:

$$P_{\text{Joint}} = \text{cat} (P_J, P_B, \text{dim} = 1), P_{\text{Joint}} \in \mathbb{R}^{Times \times 2D \times N} \quad (16)$$

$$P'_B = P_{\sigma(Times)} \quad (17)$$

$$P_{\text{marginal}} = \text{cat} (P_J, P'_B, \text{dim} = 1), P_{\text{marginal}} \in \mathbb{R}^{Times \times 2D \times N} \quad (18)$$

$$t = \text{FC} (\text{LSTM} (P_{\text{Joint}})) \quad (19)$$

$$et = \exp (\text{FC} (\text{LSTM} (P_{\text{marginal}}))) \quad (20)$$

$$mi\_lb = \bar{t} - \log \bar{et} \quad (21)$$

Due to the symmetry of mutual information, the mutual information computed pairwise among four groups can be obtained by six calculations, forming a symmetric matrix  $MI$  stacked with zeros in the middle.  $MI = \begin{bmatrix} 0 & \cdots & mi\_lb_{jb} \\ \vdots & \ddots & \vdots \\ mi\_lb_{bj} & \cdots & 0 \end{bmatrix}$ . After normalization, we obtain the mutual information weight matrix. Multiplying this matrix with the original spike-form features results in the fused features.

$$MI_{\text{av}} = \text{sum}(MI, \text{dim} = 1) / \text{sum}(MI) \quad (22)$$

$$W = (MI_{av} - \min MI_{av}) / (\max MI_{av} - \min MI_{av}) \quad (23)$$

$$P_{\text{fuse}} = W * [P_B, P_J, P_{BM}, P_{JM}]^T \quad (24)$$

$P_{\text{fuse}} \in \mathbb{R}^{\text{Times} \times D \times N}$  is then fed into the core of the MK-SGN.

### Knowledge Distillation of GCN-to-SGN

To utilize the capabilities of multimodal GCN, we propose a distillation method with GCN as the teacher and SGN as the student. Our method fully exploits the rich knowledge and representation power of pre-trained multimodal GCNs. It enhances the accuracy of the SGN without increasing computational complexity and energy consumption.

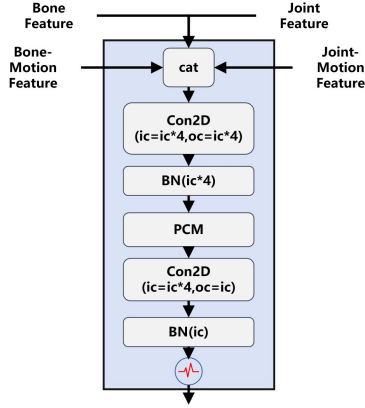


Figure 3: Feature Translation Module

**Soft label distillation** For the GCN network, we select a CTR-GCN with a 4-stream structure as the teacher network. In the teacher network, we use skeleton, joint, skeleton-motion and joint-motion data as multi-modal data sources. We input them separately into the single-stream CTR-GCN to obtain single-modal soft labels, denoted as  $y_b$ ,  $y_j$ ,  $y_{bm}$  and  $y_{jm}$ , respectively. Finally, we combine the classification results from each modality to form the multi-modal teacher soft labels  $\hat{y}$ .

$$\hat{y} = \alpha_b y_b + \alpha_j y_j + \alpha_{bm} y_{bm} + \alpha_{jm} y_{jm} \quad (25)$$

where  $\alpha_b, \alpha_j, \alpha_{bm}$  and  $\alpha_{jm}$  are hyper-parameters. Then, the final learning objective is written as:

$$L_{sdk} = \|y - \hat{y}\| \quad (26)$$

**Inner-layer feature distillation** The inner-layer features of heterogeneous GCN and SGN models differ, with GCN typically dealing with continuous decimal values, whereas SGN uses discrete spike sequences. We propose the Feature Translation Module (FTM) to address this issue, as shown in Figure 3. GCN typically deals with continuous decimal values, whereas SGN uses discrete spike sequences. To address this, we propose the Feature Translation Module (FTM), as shown in Figure 3. This learnable module effectively converts the continuous inner-layer features of GCN into spike-form features suitable for SGN. FTM first concatenates multimodal features along the channel dimension and then fuses

them using depth-wise separable convolution. Continuous features are then encoded using the PCM module. Finally, Conv2D, BN, and SN are employed to obtain spike-form features. The teacher GCN architecture typically comprises 10 GC-TC (Graph Convolution- Temporal Convolution) units. The ic is inter-channel, and the oc is outer-channel. The student GCN architecture typically comprises 10 units of SGC-STC (Spiking Graph Convolution - Spiking Temporal Convolution). We choose to leverage intermediate-level features  $T_{Ab5}, T_{Aj5}, T_{Abm5}, T_{Ajm5} \in \mathbb{R}^{2C \times \frac{T}{2} \times V}$  and high-level features  $T_{Ab8}, T_{Aj8}, T_{Abm8}, T_{Ajm8} \in \mathbb{R}^{4C \times \frac{T}{4} \times V}$  as guiding teachers in the learning process. This choice is motivated by the expansion of channel numbers and changes in the TCN network’s stride within these layers. These layers capture diverse temporal relationships and potentially capture richer feature information. We take the intermediate 5th-layer as an example, and the process is as follows:

$$T_{Am5} = \text{BN}(\text{Con2d}(\text{cat}(T_{Ab5}, T_{Aj5}, T_{Abm5}, T_{Ajm5}))) \quad (27)$$

where  $T_{Am5} \in \mathbb{R}^{8C \times \frac{T}{2} \times V}$  are fused multi-modal teacher features.

$$T_{Sm5} = \text{SN}(\text{BN}(\text{Con2d}(\text{PCM}(T_{Am5})))) \quad (28)$$

, where  $T_{Sm5} \in \mathbb{R}^{\text{Times} \times D \times V}$  are teacher spike-form feature. Similarly, we calculate the spike-form feature for the high-level layer  $T_{Sm8}$ . To guide the student network with the teacher’s pulse features, we employ cosine similarity as the loss function to measure the discrepancy between each pair of feature vectors.

$$L_{\text{fk}d_1} = \frac{1}{J} \sum_{j=1}^J \left( 1 - \frac{T_{Sm5}^j \cdot S_3^j}{\|T_{Sm5}^j\| \cdot \|S_3^j\|} \right) \quad (29)$$

$$L_{\text{fk}d_2} = \frac{1}{J} \sum_{j=1}^J \left( 1 - \frac{T_{Sm8}^j \cdot S_5^j}{\|T_{Sm8}^j\| \cdot \|S_5^j\|} \right) \quad (30)$$

$S_3$  are the spike-form feature of the 3th lay of SGN and  $S_5$  are the 5th.  $K$  is the number of action classes. And inner-layer feature distillation loss is written as:

$$L_{\text{fk}d} = \beta_1 L_{\text{fk}d_1} + \beta_2 L_{\text{fk}d_2} \quad (31)$$

where  $\beta_1$  and  $\beta_2$  are hyper-parameters. This aims to drive the student network features closer to the teacher features while optimizing the FTM for feature translation. In the end, the final learning objective with hyper-parameters  $\gamma_1, \gamma_2$  and  $\gamma_3$  is re-written as

$$L = \gamma_1 L_b + \gamma_2 L_{sdk} + \gamma_3 L_{\text{fk}d} \quad (32)$$

## EXPERIMENTS

In this section, we evaluate the classification performance of MK-SGN on skeletal action recognition datasets, e.g., NTU-RGB+D 60, NTU-RGB+D 120, NW-UCLA(Shahroudy et al. 2016; Liu et al. 2019; Wang et al. 2014). To verify the effectiveness and efficiency of the proposed model, we first replace the activation layers of the classic ST-GCN model

Table 1: Evaluation on NTU-RGB+D. Param refers to the number of parameters. Power is the average theoretical energy consumption when predicting a skeleton from the NTU-RGB+D test set, whose calculation details are shown as Equation(35), Equation(36), and Equation(37).

Method	Architecture	Param (M)	Time Step	Modal Number	Knowledge Distillation	SOPs (G)	FLOPs (G)	Power ( <i>mJ</i> )	Ntu-RGB+D 60 XSub(%)	XView(%)
ANN	(10-layer)ST-GCN (Yan, Xiong, and Lin 2018)	2.11	/	1	/	/	2.56	11.78	81.5	88.3
SNN	(10-layer)Base-SGN*	2.07	4	1	/	0.60	7.17	0.536	64.2	71.3
	(6-layer)Spikformer <sup>ICLR 2023</sup> (Zhou et al. 2022)	4.78	4	1	/	1.69	24.07	2.17	73.9	80.6
	<b>(6-layer) MK-SGN</b>	1.89	4	1	/	0.64	7.32	0.573	74.5	80.9
	<b>(6-layer) MK-SGN</b>	1.89	4	1	✓	0.66	7.65	0.582	75.9	82.1
	<b>(6-layer) MK-SGN</b>	2.17	4	4	/	0.67	7.76	0.596	76.1	82.6
	<b>(6-layer) MK-SGN</b>	2.17	4	4	✓	<b>0.68</b>	7.84	<b>0.614</b>	<b>78.5</b>	<b>85.6</b>

with LIF. This modified model, called Base-SGN\*, is then trained and tested for comparison. Based on this, we conduct ablation and comparison experiments for MK-SGN. More details on the training, datasets, hyper-parameter settings, convergence analysis, and trainable parameter analysis can be found in the Appendix.

### Ablation Study

To analyze the energy efficiency of our proposed MK-SGN and further assess the effectiveness of each component in the model, we employ theoretical formulas to evaluate the number of operations (OPs) required for classifying a single sample. Specifically, we first calculate the floating-point operations (FLOPs) for ANN, as well as the FLOPs for SNN on traditional GPUs and the theoretical synaptic operations (SOPs) on neuromorphic hardware. Based on these OPs, we further calculate the energy consumption per action sample during the testing phase. The details of SOPs and the theoretical energy calculations can be found in the Appendix. Finally, we analyze the classification accuracy through all experimental ablation studies conducted on the NTU RGB+D 60 dataset, as shown in Table 1.

**Base-SGN\*** First, we validate the effectiveness of Base-SGN\* as the foundation for the ablation study. We use the trained model and compare it with the traditional ST-GCN. We calculate the theoretical number of operations (OPs) and energy consumption. The results show that Base-SGN reduces the theoretical energy consumption by  $0.536mJ$  per action sample. However, this increases the FLOPs and decreases the accuracy to 64.2% and 71.3%. This indicates that simply replacing the activation layer is insufficient to maintain high classification accuracy.

**MK-SGC** Building on Base-SGN\*, we compare it with our proposed MK-SGN. Even without knowledge distillation, the single-modality MK-SGN achieves a notable accuracy improvement of 10.1% and 8.9% with only a minimal increase in OPs and theoretical power consumption. It also reduces the parameter count by over 50%, and decreases FLOPs and theoretical energy consumption by more than 70% compared to similar structures like Spikformer. Additionally, MK-SGN improves accuracy by 0.6% and 0.3% in comparison.

**SMF** In the case of late fusion in a multi-modal classification network, where  $n$  represents the number of modalities when classifying a single action sample, it must undergo testing for  $n$  times, leading to a theoretical energy consumption expanded to  $n$  times the original. Taking ST-GCN as an example, its theoretical OPs will become  $4 \times 2.56G$  and the Power will become  $4 \times 11.78mJ$ . To validate that our designed SMF can avoid the increased energy consumption caused by late fusion and improve accuracy, we compare the performance of multi-modal fusion with single-modal fusion. This approach avoids the increased energy consumption caused by late fusion. The theoretical energy consumption increased to  $0.67 mJ$  per action sample. And it improves the model’s accuracy by 1.6% and 1.7%

**Knowledge Distillation** We compare the accuracy of models trained with and without teacher guidance. We observe their OPs and Power to evaluate the impact of our proposed knowledge distillation method. The accuracy of SGN models trained with teacher guidance shows a noticeable improvement of 1.4% and 1.2%. At the same time, OPs and Power exhibit slight fluctuations (due to differences in the firing rates of spiking neural networks), with no significant increase observed.

**Integrated Module Performance Comparison** We carefully examine the contribution of each component, as shown in Table 1. The final MK-SGN, integrating all modules, achieves accuracies of 78.5% and 85.6%. With a Time Step of 4, compared to Spikformer, MK-SGN reduces parameter count by 54.60% and FLOPs by 67.4%, making it easier to train on traditional GPUs. Additionally, MK-SGN decreases SOPs by 59.76% and theoretical energy consumption by 71.7%, while improving accuracy by 4.6% and 5.0%, demonstrating its high performance with low energy consumption. Compared to Base-SGN, MK-SGN shows accuracy improvements of 14.3% and 11.3%. When compared to the classic ANN model ST-GCN, MK-SGN reduces energy consumption by 94.78% while maintaining similar accuracy.

### Experimental Results

We compare our proposed SGN approach with the current state-of-the-art (SOTA) ANNs and SNNs. We particularly



Table 2: Comparative results on NTU RGB+D 60 and 120. We evaluate our model in terms of classification accuracy (%). X-Sub and X-View represent cross-subject and cross-view splits.

Method	Architecture	Performance			Accuracy (%)			
		Param (M)	OPs (G)	Power (mJ)	Xsub (60)	Xview (60)	Xsub (120)	Xview (120)
ANN	Lie Group (Veeriah, Zhuang, and Qi 2015)	/	/	/	50.1	52.8	/	/
	HBRNN (Du, Wang, and Wang 2015)	/	/	/	59.1	64.0	/	/
	Deep LSTM (Shahroudy et al. 2016)	/	/	/	60.7	67.3	/	/
	ST-GCN (Yan, Xiong, and Lin 2018)	2.11	2.56	11.78	81.5	88.3	70.7	73.2
	2S-AGCN (Shi et al. 2019b)	3.48	35.8	164.68	89.2	95.0	82.9	84.9
	Shift-GCN (Cheng et al. 2020)	/	10	46	90.7	96.5	85.9	87.6
	MS-G3D (Ke et al. 2018)	3.19	67.63	311.09	91.5	96.2	86.9	88.4
	CTR-GCN (Chen et al. 2021a)	1.46	7.88	36.25	92.4	96.8	88.9	90.6
SNN	Base-SGN*	2.07	0.60	0.536	64.2	71.3	45.2	47.3
	Spikformer (Zhou et al. 2022) <sup>ICLR 2023</sup>	4.78	1.69	2.17	73.9	80.1	61.7	63.7
	Spike-driven Transformer (Yao et al. 2024) <sup>NIPS2023</sup>	4.77	1.57	1.93	73.4	80.6	62.3	64.1
	<b>MK-SGN(Ours)</b>	2.17	<b>0.68</b>	<b>0.614</b>	<b>78.5</b>	<b>85.6</b>	<b>67.8</b>	<b>69.5</b>

Table 3: Comparative results on NW-UCLA. We evaluate our model in terms of classification accuracy (%). X-Sub and X-Set represent cross-subject and cross-setup splits

Architecture (ANN/SNN)	Param (M)	OPs (G)	Power (mJ)	Acc (%)
Lie Group (Veeriah, Zhuang, and Qi 2015)	-	-	-	74.2
Actionlet ensemble (Wang et al. 2013)	-	-	-	76.0
HBRNN-L (Du, Wang, and Wang 2015)	-	-	-	78.5
Ensemble TS-LSTM (Lee et al. 2017)	-	-	-	89.2
Shift-GCN (Cheng et al. 2020)	-	0.7	3.22	94.6
CTR-GCN (Chen et al. 2021a)	1.46	2.48	12.15	96.5
Base-SGN*	2.07	0.151	0.195	86.4
Spikformer <sup>ICLR 2023</sup> (Zhou et al. 2022)	4.78	0.513	0.673	85.4
Spike-driven Transformer <sup>NIPS2023</sup> (Yao et al. 2024)	4.77	0.501	0.643	83.4
<b>MK-SGN (Ours)</b>	<b>2.17</b>	<b>0.165</b>	<b>0.207</b>	<b>92.3</b>

focus on two key performance metrics: the number of operations (OPs) and the theoretical energy consumption—in Table 2 and Table 3. To make fair comparisons, in both tables, the results of existing multi-modal GCN methods of four modalities, i.e., joint, bone, joint motion, and bone motion, are fused. The softmax scores of multiple streams are added to obtain the fused score. Their OPs and theoretical energy consumption are calculated by multiplying the corresponding value of a single flow by the number of modal flows.

We report the results of the 6-layer MK-SGN. MK-SGN achieves significantly higher accuracy on the NTU RGB+D 60,120 dataset than previous non-GCN ANN models (Veeriah, Zhuang, and Qi 2015; Du, Wang, and Wang 2015;

Shahroudy et al. 2016). On the NW-UCLA dataset, our model achieved an accuracy of 92.3%, demonstrating our approach’s effectiveness.

We also compared our model with two state-of-the-art SNN networks on all datasets. These networks lack validation for skeleton-based action recognition. To ensure a fair comparison, we applied the same training methods and epochs with similar layer structures and hidden dimensions. The results show that, with a 54.5% reduction in the number of parameters, our model achieves approximately a 5% improvement in accuracy, proving our superiority over SNNs in this domain. The theoretical energy consumption of our model is 0.614mJ per action sample. Compared with the 2s-AGCN method (Shi et al. 2019b), the theoretical energy consumption is reduced by 99.62%. Compared with MS-G3D, the theoretical energy consumption is reduced by 99.80%. Compared with Shift-GCN (Cheng et al. 2020) and CTR-GCN (Chen et al. 2021a), which are characterized by lightweight, the theoretical energy consumption is reduced by 98.67% and 98.31%, respectively.

These results empirically verify the advantage of MK-SGN in skeleton-based action recognition.

## Conclusion

This work introduces the Spiking Graph Convolutional Network (MK-SGN) with multimodal fusion and knowledge distillation. It is the first to combine spiking neural networks with graph convolutional networks for skeleton action recognition. Our research addresses the high energy consumption of traditional GCN methods, achieving significant performance improvements through multimodal fusion and knowledge distillation. The MK-SGN model significantly reduces energy consumption on three skeleton action recognition datasets, cutting it by over 98% compared to the best ANN methods. Additionally, it surpasses the current state-of-the-art SNN methods in accuracy, improving recognition by 5%.

## Appendix

In the appendix, we first provide a detailed introduction of the dataset, followed by the hyperparameter settings and training details. Finally, we explain the calculation methods for firing rate, operations (OPs), and theoretical energy consumption.

### Datasets

NTU-RGB+D (Shahroudy et al. 2016) is a comprehensive dataset that includes 60 action classes and 56,000 video clips, providing detailed skeleton data covering a wide range of daily activities. This dataset is widely used in the field of action recognition due to its rich variety of actions and extensive data volume. It includes 3D coordinates of 25 major body joints, captured using a Kinect v2 sensor, allowing for precise human movement modelling.

NTU-RGB+D120 (Liu et al. 2019), an extended version of the original NTU-RGB+D. The dataset significantly expands to include 120 action classes and over 114,000 video clips. This extended dataset offers even richer skeleton data, making it one of the largest and most comprehensive skeleton-based action recognition datasets available. Including a broader range of actions and a larger number of video clips provides a valuable resource for developing and evaluating advanced action recognition algorithms.

NW-UCLA (Wang et al. 2014) consists of 10 action classes and 1,494 video clips, captured from different viewpoints. This dataset provides diverse skeleton data to assess the robustness of action recognition models to viewpoint variations. The skeleton data includes 3D coordinates of 20 major body joints, challenging models to perform consistently across different perspectives.

### Hyper-Parameters Settings

In this section, we give the specific hyperparameters of the LIF model and training settings in all experiments, shown as Table 4.

Table 4: Hyper-parameter setting on LIF model.

Parameter	Value
Threshold $V_{th}$	1.0
Reset potential $V_{reset}$	0
Decay factor $\tau$	0.25
Surrogate function’s window size $a$	1.0

The models for conducting experiments are implemented based on Pytorch (Paszke et al. 2019) and SpikingJelly (Fang et al. 2023) on a server equipped with an NVIDIA SMI V100 GPU, which has 30GB of memory. We adopt the SGD optimizer with an initial learning rate of 0.1 and a weight decay rate of 0.1 for efficient parameter optimization of Base-SGN, Spikformer and Spike-driven Transformer. The batch size is set to 60 for NTU-RGB+D 60, 40 for NTU-RGB+D 120 and 120 for NW-UCLA.

We employ two SGD optimizers during our training process to fine-tune MK-SGN parameters. One optimizer is specifically used to enhance the SGN model, improving its

efficiency in handling tasks; the other optimizer is dedicated to refining the FTM, boosting the effectiveness of feature transfer from the teacher to the student model. The hyper-parameters are shown in Table 5. In the testing phase, we only evaluate the SGN model itself.

Table 5: Hyper-parameter training settings of MK-SGN.

Parameter	NTU-RGB+D	NTU-RGB+D	NW-UCLA
	60	120	
Learning Rate	0.1/0.1	0.1/0.1	0.1/0.1
Decay rate	0.1/0.1	0.1/0.1	0.1/0.1
Batch Size	60	40	120
Time Steps	4	4	4
Training Epochs	64	64	64
Step	50	50	50
Dropout Rate	0.3	0.3	0.3
Weight Decay	1e-4	1e-4	1e-4
Optimizer	SGD/SGD	SGD/SGD	SGD/SGD

### Theoretical Energy Consumption laCalculation

Referencing (Zhou et al. 2022), we must first calculate the synaptic operations(SOPs) when calculating theoretical energy consumption. To calculate the SOPs of each model, we need to calculate the fire rate of each LIF neuron. It is defined as the firing probability of each neuron per timestep and can be estimated by:

$$r = \frac{\#Spikes}{T}$$

where #Spikes denotes the number of spikes emitted by the neuron during  $T$  timesteps, and  $T$  is the duration of the time window in which spikes are counted, typically measured in milliseconds (ms). We use the firing rates of each module in MK-SGN on the NTU-RGB+D 60 dataset as a case study, shown in Table 6.

Then, according to (Kundu, Pedram, and Beerel 2021; Kundu et al. 2021; Yao et al. 2023), the theoretical energy consumption of Base-SGN and MK-SGN are calculated as:

$$SOPs(l) = fr \times Times \times FLOPs(l) \quad (33)$$

$$E_{Base-SGN} = E_{MAC} \times FL_{SNNConv}^1 + E_{AC} \times \left( \sum_{n=2}^N SOP_{SNNConv}^n + \sum_{m=1}^M SOP_{SNNFC}^m \right) \quad (34)$$

$$E_{MK-SGN} = n_m \times E_{MAC} \times FL_{SNNConv}^1 + E_{AC} \times \left( \left[ \frac{k \times (k-1)}{2} \right] SOP_{MC} + \sum_{n=n_m}^N SOP_{SNNConv}^n + \sum_{m=1}^M SOP_{SNNFC}^m + \sum_{l=1}^L SOP_{SA}^l + \sum_{i=1}^I SOP_{SGSA}^i \right) \quad (35)$$



where  $l$  is a block/layer in SGN,  $fr$  is the firing rate of the input spike train of the block/layer and  $Times$  is the simulation time step of the spiking neuron.  $FLOPs(l)$  refers to the floating point operations of  $l$ , which is the number of multiply-and-accumulate (MAC) operations. And  $SOPs$  is the number of spike-based accumulate (AC) operations.  $FL_{SNN}^1$  is the first layer to encode skeleton data into spike-form. The SOP of  $n$  SNN Conv layers,  $m$  SNN Fully Connected Layer (FC) and  $l$  SA and  $i$  SGSA are added together and multiplied by  $E_{MAC}$ . When calculating  $E_{MK-SGN}$ ,  $SOP_{MC}$  is utilized to estimate the theoretical energy consumption of fusing  $k$  modalities. We assume that the MAC and AC operations are implemented on the 45nm hardware (Zhou et al. 2022), where  $E_{MAC} = 4.6pJ$  and  $E_{AC} = 0.9pJ$ . The theoretical energy consumption of block  $b$  for ANN and SNN are as follows:

$$\text{Power}(b) = 4.6pJ \times \text{FLOPs}(b) \quad (36)$$

$$\text{Power}(b) = 0.9pJ \times \text{SOPs}(b) \quad (37)$$

### Architecture Details

The main network architectures in this study are the GCN series architecture and the SNN-based Transformer architecture. In this section, we will detail these architectures to ensure that our primary comparison experiments are fair. Specifically, we first present the architecture of traditional GCN networks, including the composition of each layer, the input and output tensor dimensions (channel dimensions), and where stride changes occur. Traditional GCNs typically have a ten-layer pyramid-shaped structure, with channel dimensions progressing from 3 to 64, then to 128, and finally to 256. When the dimensions change, a stride=2 transformation is performed on the temporal frame dimension. The final classification result is obtained through pooling layers and a fully connected (fc) layer.

Additionally, we present the structure of Base-SGN, which is designed similarly to traditional GCNs. We also showcase the proposed MK-SGN network structure, which consists of only six main layers.

We adapt the architecture of SNN-driven Transformer networks, such as Spikformer, to handle skeleton data. These networks are typically used for processing images and videos. We remove the downsampling levels in the SPS (spiking patch splitting) layer, retaining only a single SPS layer and six layers of Spiking Self-Attention and MLP for training. Additionally, we set the hidden layer dimensions to 256 to ensure fairness. Specifically, the architecture of each model is shown in Table 7.

Table 6: Layer spiking firing rates of model MK-SGN (Time Step = 4) on NTU-RGB+D

Layer	Module Name	Average Firing Rate (Times Step=4)
Fire layer	SC1_lif	0.0446
	SC2_lif	0.0865
	SC3_lif	0.0702
	SC4_lif	0.0480
Lay1	SA-SGC1_lif1	0.0123
	SA-SGC1_lif2	0.0141
	SG-SA1_lifx	0.0095
	SG-SA1_Conv1_lifq	0.0072
	SG-SA1_Conv1_lifk	0.0103
	SG-SA1_Conv1_lifv	0.0090
	SG-SA1_Conv1_lifkv	0.0108
	STC1_lif	0.0177
STC1_res_lif	0.0101	
Lay2	SA-SGC2_lif1	0.0101
	SA-SGC2_lif2	0.0078
	SG-SA2_lifx	0.0121
	SG-SA2_lifq	0.0098
	SG-SA2_lifk	0.0098
	SG-SA2_lifv	0.0091
	SG-SA2_lifkv	0.0143
STC2_lif	0.0117	
Lay3	SA-SGC3_lif1	0.0089
	SA-SGC3_lif2	0.0105
	SG-SA3_lifx	0.0121
	SG-SA3_lifq	0.0087
	SG-SA3_lifk	0.0135
	SG-SA3_lifv	0.0116
	SG-SA3_lifkv	0.0101
STC3_lif	0.0121	
STC3_res_lif	0.0091	
Lay4	SA-SGC4_lif1	0.0089
	SA-SGC4_lif3	0.0097
	SG-SA4_lifx	0.0119
	SG-SA4_lifq	0.0109
	SG-SA4_lifk	0.0093
	SG-SA4_lifv	0.0102
	SG-SA4_lifkv	0.0124
STC4_lif	0.0090	
Lay5	SA-SGC5_lif1	0.0107
	SA-SGC5_lif2	0.0119
	SG-SA5_lifx	0.0119
	SG-SA5_lifq	0.0093
	SG-SA5_lifk	0.0094
	SG-SA5_lifv	0.0103
	SG-SA5_lifkv	0.0127
STC5_lif	0.0107	
STC5_res_lif	0.0119	
Lay6	SA-SGC6_lif1	0.0093
	SA-SGC6_lif2	0.0209
	SG-SA6_lifx	0.0147
	SG-SA6_lifq	0.0141
	SG-SA6_lifk	0.0141
	SG-SA6_lifv	0.0094
SG-SA6_lifkv	0.0090	
STC6_lif	0.0150	
Head	FC_lif1	0.0163

Table 7: Model’s architecture for NTU-RGB+D 60

Layer	GCN (Input/Output)	GCN Structure Layer Composition	Base-SGN (Input/Output)	MK-SGN (Input/Output)	SGN Structure Layer Composition	Spikformer (Input/Output)	Spikformer Structure Layer Composition
Fire layer	-	-	3/3	3/3	SC-(SMF)	3/256	SPS
1	3/64	GC-TC	3/64	3/64	SGC-STC	256/256	SSA-MLP
2	64/64	GC-TC	64/64	64/64	SGC-STC	256/256	SSA-MLP
3	64/64	GC-TC	64/64	64/128(stride=2)	SGC-STC	256/256	SSA-MLP
4	64/64	GC-TC	64/64	128/128	SGC-STC	256/256	SSA-MLP
5	64/128(stride=2)	GC-TC	64/128(stride=2)	128/256(stride=2)	SGC-STC	256/256	SSA-MLP
6	128/128	GC-TC	128/128	256/256	SGC-STC	256/256	SSA-MLP
7	128/128	GC-TC	128/128	-	SGC-STC	-	-
8	128/256(stride=2)	GC-TC	128/256(stride=2)	-	SGC-STC	-	-
9	256/256	GC-TC	256/256	-	SGC-STC	-	-
10	256/256	GC-TC	256/256	-	SGC-STC	-	-
final	256/class number	GAP-FC	256/class number	256/class number	GAP-FC	256/class number	GAP-FC

## References

- Agapiou, A.; Amann, A.; Mochalski, P.; Statheropoulos, M.; and Thomas, C. L. P. 2015. Trace detection of endogenous human volatile organic compounds for search, rescue and emergency applications. *TrAC Trends in Analytical Chemistry*, 66: 158–175.
- Baltrušaitis, T.; Ahuja, C.; and Morency, L.-P. 2018. Multimodal machine learning: A survey and taxonomy. *IEEE transactions on pattern analysis and machine intelligence*, 41(2): 423–443.
- Chen, Y.; Zhang, Z.; Yuan, C.; Li, B.; Deng, Y.; and Hu, W. 2021a. Channel-wise topology refinement graph convolution for skeleton-based action recognition. 13359–13368.
- Chen, Z.; Li, S.; Yang, B.; Li, Q.; and Liu, H. 2021b. Multi-scale spatial temporal graph convolutional network for skeleton-based action recognition. 35(2): 1113–1122.
- Cheng, K.; Zhang, Y.; He, X.; Chen, W.; Cheng, J.; and Lu, H. 2020. Skeleton-based action recognition with shift graph convolutional network. 183–192.
- Chéron, G.; Laptev, I.; and Schmid, C. 2015. P-cnn: Pose-based cnn features for action recognition. 3218–3226.
- Chi, H.-g.; Ha, M. H.; Chi, S.; Lee, S. W.; Huang, Q.; and Ramani, K. 2022. Infogcn: Representation learning for human skeleton-based action recognition. 20186–20196.
- Du, Y.; Wang, W.; and Wang, L. 2015. Hierarchical recurrent neural network for skeleton based action recognition. In *Proceedings of the IEEE conference on computer vision and pattern recognition*, 1110–1118.
- Dutta, S.; Kumar, V.; Shukla, A.; Mohapatra, N. R.; and Ganguly, U. 2017. Leaky integrate and fire neuron by charge-discharge dynamics in floating-body MOSFET. *Scientific reports*, 7(1): 8257.
- Elharrouss, O.; Almaadeed, N.; and Al-Maadeed, S. 2021. A review of video surveillance systems. *Journal of Visual Communication and Image Representation*, 77: 103116.
- Fang, W.; Chen, Y.; Ding, J.; Yu, Z.; Masquelier, T.; Chen, D.; Huang, L.; Zhou, H.; Li, G.; and Tian, Y. 2023. Spiking-Jelly: An open-source machine learning infrastructure platform for spike-based intelligence. *Science Advances*, 9(40): eadi1480.
- Feng, L.; Zhao, Y.; and Zhao, W. 2022. A comparative review of graph convolutional networks for human skeleton-based action recognition. *Artificial Intelligence Review*, 1–31.
- Gao, J.; Li, P.; Chen, Z.; and Zhang, J. 2020. A survey on deep learning for multimodal data fusion. *Neural Computation*, 32(5): 829–864.
- Hu, Y.; Deng, L.; Wu, Y.; and Yao, M. 2024. Advancing Spiking Neural Networks Toward Deep Residual Learning. *IEEE Transactions on Neural Networks and Learning Systems*.
- Hu, Y.; Tang, H.; and Pan, G. 2021. Spiking deep residual networks. *IEEE Transactions on Neural Networks and Learning Systems*, 34(8): 5200–5205.
- Hu, Y.; Zheng, Q.; Jiang, X.; and Pan, G. 2023. Fast-snn: Fast spiking neural network by converting quantized ann. *IEEE Transactions on Pattern Analysis and Machine Intelligence*.
- Ke, Q.; Bennamoun, M.; An, S.; Sohel, F.; and Boussaid, F. 2018. Learning clip representations for skeleton-based 3d action recognition. *IEEE Transactions on Image Processing*, 27(6): 2842–2855.
- Kim, H.; and Mnih, A. 2018. Disentangling by factorising. 2649–2658.
- Kim, Y.; Chough, J.; and Panda, P. 2022. Beyond classification: Directly training spiking neural networks for semantic segmentation. *Neuromorphic Computing and Engineering*, 2(4): 044015.
- Kundu, S.; Datta, G.; Pedram, M.; and Beerel, P. A. 2021. Spike-thrift: Towards energy-efficient deep spiking neural networks by limiting spiking activity via attention-guided compression. In *Proceedings of the IEEE/CVF Winter Conference on Applications of Computer Vision*, 3953–3962.
- Kundu, S.; Pedram, M.; and Beerel, P. A. 2021. Hire-snn: Harnessing the inherent robustness of energy-efficient deep spiking neural networks by training with crafted input noise. In *Proceedings of the IEEE/CVF International Conference on Computer Vision*, 5209–5218.
- Lee, C.; Sarwar, S. S.; Panda, P.; Srinivasan, G.; and Roy, K. 2020a. Enabling spike-based backpropagation for training deep neural network architectures. *Frontiers in neuroscience*, 14: 497482.
- Lee, C.; Sarwar, S. S.; Panda, P.; Srinivasan, G.; and Roy, K. 2020b. Enabling spike-based backpropagation for training deep neural network architectures. *Frontiers in neuroscience*, 14: 497482.
- Lee, I.; Kim, D.; Kang, S.; and Lee, S. 2017. Ensemble deep learning for skeleton-based action recognition using temporal sliding lstm networks. In *Proceedings of the IEEE international conference on computer vision*, 1012–1020.
- Lee, J. H.; Delbruck, T.; and Pfeiffer, M. 2016. Training deep spiking neural networks using backpropagation. *Frontiers in neuroscience*, 10: 228000.
- Li, B.; Li, X.; Zhang, Z.; and Wu, F. 2019a. Spatio-temporal graph routing for skeleton-based action recognition. 33(01): 8561–8568.
- Li, M.; Chen, S.; Chen, X.; Zhang, Y.; Wang, Y.; and Tian, Q. 2019b. Actional-structural graph convolutional networks for skeleton-based action recognition. 3595–3603.
- Lin, Y.; Hu, Y.; Ma, S.; Yu, D.; and Li, G. 2022. Rethinking pretraining as a bridge from anns to snns. *IEEE Transactions on Neural Networks and Learning Systems*.
- Liu, J.; Shahroudy, A.; Perez, M.; Wang, G.; Duan, L.-Y.; and Kot, A. C. 2019. Ntu rgb+ d 120: A large-scale benchmark for 3d human activity understanding. *IEEE transactions on pattern analysis and machine intelligence*, 42(10): 2684–2701.
- Liu, J.; Shahroudy, A.; Xu, D.; and Wang, G. 2016. Spatio-temporal lstm with trust gates for 3d human action recognition. In *Computer Vision—ECCV 2016: 14th European Con-*

- ference, Amsterdam, The Netherlands, October 11-14, 2016, *Proceedings, Part III 14*, 816–833. Springer.
- Liu, J.; Wang, G.; Hu, P.; Duan, L.-Y.; and Kot, A. C. 2017. Global context-aware attention lstm networks for 3d action recognition. 1647–1656.
- Liu, M.; Liu, H.; and Chen, C. 2017. Enhanced skeleton visualization for view invariant human action recognition. *Pattern Recognition*, 68: 346–362.
- Liu, Z.; Zhang, H.; Chen, Z.; Wang, Z.; and Ouyang, W. 2020. Disentangling and unifying graph convolutions for skeleton-based action recognition. 143–152.
- Lotfi Rezaabad, A.; and Vishwanath, S. 2020. Long short-term memory spiking networks and their applications. 1–9.
- Nwakanma, C. I.; Islam, F. B.; Maharani, M. P.; Kim, D.-S.; and Lee, J.-M. 2021. Iot-based vibration sensor data collection and emergency detection classification using long short term memory (lstm). 273–278.
- Paszke, A.; Gross, S.; Massa, F.; Lerer, A.; Bradbury, J.; Chanan, G.; Killeen, T.; Lin, Z.; Gimelshein, N.; Antiga, L.; et al. 2019. Pytorch: An imperative style, high-performance deep learning library. *Advances in neural information processing systems*, 32.
- Roy, K.; Jaiswal, A.; and Panda, P. 2019. Towards spike-based machine intelligence with neuromorphic computing. *Nature*, 575(7784): 607–617.
- Shahroudy, A.; Liu, J.; Ng, T.-T.; and Wang, G. 2016. Ntu rgb+d: A large scale dataset for 3d human activity analysis. 1010–1019.
- Sheridan, T. B. 2016. Human–robot interaction: status and challenges. *Human factors*, 58(4): 525–532.
- Shi, L.; Zhang, Y.; Cheng, J.; and Lu, H. 2019a. Skeleton-based action recognition with directed graph neural networks. 7912–7921.
- Shi, L.; Zhang, Y.; Cheng, J.; and Lu, H. 2019b. Two-stream adaptive graph convolutional networks for skeleton-based action recognition. In *Proceedings of the IEEE/CVF conference on computer vision and pattern recognition*, 12026–12035.
- Shrestha, S. B.; and Orchard, G. 2018. Slayer: Spike layer error reassignment in time. *Advances in neural information processing systems*, 31.
- Song, S.; Lan, C.; and Xing, J. 2017. An end-to-end spatio-temporal attention model for human action recognition from skeleton data. In *Proceedings of the AAAI conference on artificial intelligence*, volume 31.
- Stromatias, E.; Soto, M.; Serrano-Gotarredona, T.; and Linares-Barranco, B. 2017. An event-driven classifier for spiking neural networks fed with synthetic or dynamic vision sensor data. *Frontiers in neuroscience*, 11: 269013.
- Tavanaei, A.; Ghodrati, M.; Kheradpisheh, S. R.; Masquelier, T.; and Maida, A. 2019. Deep learning in spiking neural networks. *Neural networks*, 111: 47–63.
- Veeriah, V.; Zhuang, N.; and Qi, G.-J. 2015. Differential recurrent neural networks for action recognition. 4041–4049.
- Wang, H.; and Wang, L. 2017. Modeling temporal dynamics and spatial configurations of actions using two-stream recurrent neural networks. 499–508.
- Wang, J.; Liu, Z.; Wu, Y.; and Yuan, J. 2013. Learning actionlet ensemble for 3D human action recognition. *IEEE transactions on pattern analysis and machine intelligence*, 36(5): 914–927.
- Wang, J.; Nie, X.; Xia, Y.; Wu, Y.; and Zhu, S.-C. 2014. Cross-view action modeling, learning and recognition. In *Proceedings of the IEEE conference on computer vision and pattern recognition*, 2649–2656.
- Wang, Y.; Wu, Y.; Tang, S.; He, W.; Guo, X.; Zhu, F.; Bai, L.; Zhao, R.; Wu, J.; He, T.; et al. 2023. Hulk: A Universal Knowledge Translator for Human-Centric Tasks. *arXiv preprint arXiv:2312.01697*.
- Wu, Y.; Deng, L.; Li, G.; and Shi, L. 2018. Spatio-temporal backpropagation for training high-performance spiking neural networks. *Frontiers in neuroscience*, 12: 323875.
- Xiao, M.; Meng, Q.; Zhang, Z.; Wang, Y.; and Lin, Z. 2021. Training feedback spiking neural networks by implicit differentiation on the equilibrium state. *Advances in neural information processing systems*, 34: 14516–14528.
- Yan, S.; Xiong, Y.; and Lin, D. 2018. Spatial temporal graph convolutional networks for skeleton-based action recognition. In *Proceedings of the AAAI conference on artificial intelligence*, volume 32.
- Yang, S.; Wang, X.; Gao, L.; and Song, J. 2022. Mkegcn: Multi-modal knowledge embedded graph convolutional network for skeleton-based action recognition in the wild. In *2022 IEEE International Conference on Multimedia and Expo (ICME)*, 01–06. IEEE.
- Yao, M.; Gao, H.; Zhao, G.; Wang, D.; Lin, Y.; Yang, Z.; and Li, G. 2021. Temporal-wise attention spiking neural networks for event streams classification. In *Proceedings of the IEEE/CVF International Conference on Computer Vision*, 10221–10230.
- Yao, M.; Hu, J.; Zhou, Z.; Yuan, L.; and Tian, Y. 2024. Spike-driven transformer. *Advances in Neural Information Processing Systems*, 36.
- Yao, M.; Zhao, G.; Zhang, H.; Hu, Y.; Deng, L.; Tian, Y.; Xu, B.; and Li, G. 2023. Attention spiking neural networks. *IEEE transactions on pattern analysis and machine intelligence*.
- Zhang, J.; Dong, B.; Zhang, H.; Ding, J.; Heide, F.; Yin, B.; and Yang, X. 2022. Spiking transformers for event-based single object tracking. 8801–8810.
- Zhou, Z.; Zhu, Y.; He, C.; Wang, Y.; Yan, S.; Tian, Y.; and Yuan, L. 2022. Spikformer: When spiking neural network meets transformer. *arXiv preprint arXiv:2209.15425*.
- Zhu, Z.; Peng, J.; Li, J.; Chen, L.; Yu, Q.; and Luo, S. 2022. Spiking graph convolutional networks. *arXiv preprint arXiv:2205.02767*.

## Reproducibility Checklist

This paper Includes a conceptual outline and/or pseudocode description of AI methods introduced (yes) Clearly delineates statements that are opinions, hypothesis, and speculation from objective facts and results (yes) Provides well marked pedagogical references for less-familiare readers to gain background necessary to replicate the paper (yes) Does this paper make theoretical contributions? (yes)

If yes, please complete the list below.

All assumptions and restrictions are stated clearly and formally. (yes) All novel claims are stated formally (e.g., in theorem statements). (yes) Proofs of all novel claims are included. (yes) Proof sketches or intuitions are given for complex and/or novel results. (yes) Appropriate citations to theoretical tools used are given. (yes) All theoretical claims are demonstrated empirically to hold. (yes) All experimental code used to eliminate or disprove claims is included. (NA) Does this paper rely on one or more datasets? (yes)

If yes, please complete the list below.

A motivation is given for why the experiments are conducted on the selected datasets (yes) All novel datasets introduced in this paper are included in a data appendix. (NA) All novel datasets introduced in this paper will be made publicly available upon publication of the paper with a license that allows free usage for research purposes. (NA) All datasets drawn from the existing literature (potentially including authors' own previously published work) are accompanied by appropriate citations. (yes) All datasets drawn from the existing literature (potentially including authors' own previously published work) are publicly available. (yes) All datasets that are not publicly available are described in detail, with explanation why publicly available alternatives are not scientifically satisfying. (NA) Does this paper include computational experiments? (yes)

If yes, please complete the list below.

Any code required for pre-processing data is included in the appendix. (no). All source code required for conducting and analyzing the experiments is included in a code appendix. (no) All source code required for conducting and analyzing the experiments will be made publicly available upon publication of the paper with a license that allows free usage for research purposes. (yes) All source code implementing new methods have comments detailing the implementation, with references to the paper where each step comes from (yes) If an algorithm depends on randomness, then the method used for setting seeds is described in a way sufficient to allow replication of results. (NA) This paper specifies the computing infrastructure used for running experiments (hardware and software), including GPU/CPU models; amount of memory; operating system; names and versions of relevant software libraries and frameworks. (yes) This paper formally describes evaluation metrics used and explains the motivation for choosing these metrics. (yes) This paper states the number of algorithm runs used to compute each reported result. (yes) Analysis of experiments goes beyond single-dimensional summaries of performance (e.g., average; median) to include measures of variation, confidence, or other distributional information. (yes) The significance of any improvement or de-

crease in performance is judged using appropriate statistical tests (e.g., Wilcoxon signed-rank). (yes) This paper lists all final (hyper-)parameters used for each model/algorithm in the paper's experiments. (yes) This paper states the number and range of values tried per (hyper-) parameter during development of the paper, along with the criterion used for selecting the final parameter setting. (partial)